



This is a repository copy of *Application of Binary Permeability Fields for the Study of CO<sub>2</sub> Leakage from Geological Carbon Storage in Saline Aquifers of the Michigan Basin*.

White Rose Research Online URL for this paper:

<https://eprints.whiterose.ac.uk/123180/>

Version: Accepted Version

---

**Article:**

González-Nicolás, A., Bau, D. [orcid.org/0000-0002-0730-5478](https://orcid.org/0000-0002-0730-5478) and Cody, B.M. (2018) Application of Binary Permeability Fields for the Study of CO<sub>2</sub> Leakage from Geological Carbon Storage in Saline Aquifers of the Michigan Basin. *Mathematical Geosciences*, 50 (5). pp. 525-547. ISSN 1874-8961

<https://doi.org/10.1007/s11004-017-9706-x>

---

**Reuse**

Items deposited in White Rose Research Online are protected by copyright, with all rights reserved unless indicated otherwise. They may be downloaded and/or printed for private study, or other acts as permitted by national copyright laws. The publisher or other rights holders may allow further reproduction and re-use of the full text version. This is indicated by the licence information on the White Rose Research Online record for the item.

**Takedown**

If you consider content in White Rose Research Online to be in breach of UK law, please notify us by emailing [eprints@whiterose.ac.uk](mailto:eprints@whiterose.ac.uk) including the URL of the record and the reason for the withdrawal request.



[eprints@whiterose.ac.uk](mailto:eprints@whiterose.ac.uk)  
<https://eprints.whiterose.ac.uk/>

1 Application of Binary Permeability Fields for the Study of CO<sub>2</sub> Leakage  
2 from Geological Carbon Storage in Saline Aquifers of the Michigan Basin<sup>1</sup>

3

4 Ana González-Nicolás<sup>1,2,\*</sup>, Domenico Baù<sup>3</sup>, Brent M. Cody<sup>4</sup>

5

6 <sup>1</sup>Energy Geosciences Division, Lawrence Berkeley National Laboratory, University of  
7 California, Berkeley, CA, USA

8 <sup>2</sup>Now at Institute for Modelling Hydraulic and Environmental Systems (LS<sup>3</sup>)/SimTech,  
9 University of Stuttgart, Stuttgart, Germany

10 <sup>3</sup>University of Sheffield, Department of Civil and Structural Engineering, Sheffield, UK,

11 <sup>4</sup>Natural Resources Consulting Engineers Inc., Fort Collins, CO, USA

12

13 \*Corresponding author: T: +49 711 685-60109

14 Mail address: Institute for Modelling Hydraulic and Environmental Systems (LS3)/SimTech  
15 Pfaffenwaldring 5a, D-70569 Stuttgart

16 E-mail address: anagna@gmail.com (A. González-Nicolás)

17 orcid iD 0000-0003-2869-8255

18

19 **Abstract**

20 The feasibility of geological carbon storage sites depends on their capacity to safely retain  
21 CO<sub>2</sub>. While deep saline formations and depleted gas/oil reservoirs are good candidates to  
22 sequester CO<sub>2</sub>, gas/oil reservoirs typically have a limited storage capacity (~1 Mt/year) compared  
23 to alternative targets considered for CO<sub>2</sub> disposal (Celia et al. 2015). In this respect, deep saline  
24 aquifers are considered more appropriate formations for geological carbon storage but present the  
25 disadvantage of having limited characterization data. In particular, information about the

---

<sup>1</sup> Accepted for publication in Mathematical Geoscience (DOI 10.1007/s11004-017-9706-x).  
Available online [here](#).

26 continuity of the overlying sealing formations (caprock) is often sparse if it exists at all. In this  
27 work, a study of CO<sub>2</sub> leakage is conducted for a candidate geological carbon storage (GCS) site  
28 located in the Michigan Basin, whose sealing properties of the caprock are practically unknown.  
29 Quantification of uncertainty on CO<sub>2</sub> leakage from the storage formation is achieved through a  
30 Monte Carlo simulation approach, relying on the use of a computationally efficient semi-  
31 analytical leakage model based upon the solution derived by Nordbotten et al. (2009), which  
32 assumes leakage occurs across “passive” wells intersecting caprock layers. A categorical indicator  
33 Kriging simulator is developed and implemented to represent the caprock sealing properties and  
34 model the permeability uncertainty. Binary fields of caprock permeability are generated and  
35 exhibit mostly low permeability, with sparsely-occurring local high permeability areas where  
36 brine and CO<sub>2</sub> may leak out of the storage formation. In addition, the feasibility of extending the  
37 use of the semi-analytical model to large-area leakage pathways is studied. This work advances a  
38 methodology for preliminary uncertainty quantification of CO<sub>2</sub> leakage at sites of GCS with little  
39 or no information on the sealing properties of the caprock. The implemented analysis shows that,  
40 for the considered site, CO<sub>2</sub> leakage may not be negligible even for relatively low (~1%)  
41 probabilities of finding permeable inclusions in the caprock and highlights the importance of  
42 being able to characterize caprock sealing properties over large areas.

43 **Keywords:** Categorical indicator Kriging simulator; CO<sub>2</sub> leakage; CO<sub>2</sub> storage; Semi-analytical  
44 solution.

## 45 **1 Introduction**

46 Increases in average global air and ocean temperatures are documented around the world  
47 with a global mean annual surface temperature increase of 0.3-0.6°C since the late 19<sup>th</sup> century  
48 (Nicholls et al. 1996). This phenomenon is due to the proliferation of greenhouse gas  
49 concentrations from anthropogenic emissions, particularly from carbon dioxide (CO<sub>2</sub>), the most  
50 important greenhouse gas produced by human activities (IPCC 2007). To stabilize CO<sub>2</sub> emissions  
51 into the atmosphere several strategies have been suggested, among them geological carbon  
52 storage (GCS). GCS is advanced as a promising approach to reduce CO<sub>2</sub> emissions from power

53 plants without needing to switch fuel sources (IPCC 2005). Suitable reservoirs for GCS are deep  
54 saline formations, depleted oil and gas reservoirs, and unmineable coal seams (Bergman and  
55 Winter 1995; Bachu 2003; Ruether 1998). Deep saline formations are widespread and offer 60%  
56 of the estimated storage capacity (IEA 2008). However, compared to oil and gas reservoirs, they  
57 lack characterization data and available information about their geological properties is usually  
58 scarce.

59         One of the requirements for GCS is the presence of a sealing formation that prevents  
60 stored CO<sub>2</sub> from escaping from the injected formation (IPCC 2005) and guarantees a long term  
61 sequestration. Deep saline aquifers have the inconvenience of being typically unexplored.  
62 Accordingly, little is known about the properties of the sealing formations, which are potentially  
63 compromised by the presence of leakage pathways, such as faults or fractures, permeable areas  
64 of the caprock, and poorly completed existing wells (IPCC 2005).

65         Several studies that investigate the importance of CO<sub>2</sub> leakage associated with faults and  
66 existing wells have been documented. For instance, Chang et al. (2008) studied the CO<sub>2</sub> leakage  
67 through faults where flow properties of faults are uncertain. They found that lateral CO<sub>2</sub> migration  
68 through overlying permeable formations attenuates CO<sub>2</sub> leakage through faults. The effect of  
69 faults, fault permeability, and flow velocity of groundwater on the migration of a CO<sub>2</sub> plume was  
70 studied by Sakamoto et al. (2011). Zhang et al. (2010) proposed a method to calculate the  
71 probability of CO<sub>2</sub> leakage through fractures and faults in a two-dimensional system. In high well-  
72 density areas, abandoned wells may represent a significant escape pathway for the injected CO<sub>2</sub>.  
73 Gasda et al. (2004) observed that a CO<sub>2</sub> plume could impact twenty to several hundred abandoned  
74 wells depending on the well density. Kopp et al. (2010) concluded that high risk of leakage  
75 through abandoned wells was produced by long injection times, small distances between injection  
76 wells and leaky wells, high permeability anisotropy, high geothermal gradient, and low depth. In  
77 Celia et al. (2011), the permeability of abandoned wells was identified as the most influential  
78 parameter resulting in CO<sub>2</sub> leakage from GCS. Noguees et al. (2012) implemented a Monte Carlo  
79 simulation where the main uncertainty was the effective well permeability. They showed that  
80 results on leakage depended on formation properties, location, and number of leaky wells.

81 In González-Nicolás et al. (2015a), stochastic and global sensitivity analyses were  
82 applied to study different types of uncertainty affecting leakage of CO<sub>2</sub> through passive wells  
83 during GCS operations for a potential candidate site located in the Michigan Basin. In this work,  
84 the investigation of González-Nicolás et al. (2015a) is extended to include the presence of  
85 potential areas of high permeability of the caprock potentially much larger than passive wells.  
86 The level of uncertainty is significantly increased since the location of passive wells is known,  
87 whereas the location, the size and the spatial frequency of caprock discontinuities are practically  
88 unknown. A probabilistic study of CO<sub>2</sub> leakage is performed by applying a Monte Carlo  
89 simulation approach, where the main source of uncertainty is the caprock permeability. “Weak”  
90 areas of the sealing formation are herein considered as localized depositions of higher  
91 permeability materials and referred to as “inclusions”.

92 A categorical indicator Kriging simulation algorithm is applied to generate ensembles of  
93 realizations of the caprock permeability field with two types of facies: 1) sealing formation (areas  
94 with low permeability), and 2) inclusions (areas with high permeability). The caprock  
95 permeability ensemble is thus used in a Monte Carlo analysis to perform a stochastic simulation  
96 of CO<sub>2</sub> injection and probabilistically quantify leakage through the weak caprock areas. Due to  
97 the unavailability of geological data with sufficient resolution, different geostatistical  
98 configurations for the sealing formation are studied to assess the impact of the uncertainty of  
99 caprock inclusions on the probability of CO<sub>2</sub> leakage. Areas of high permeability having relatively  
100 similar spatial locations are grouped together into clusters to reduce the number of leaky points  
101 used by the semi-analytical multiphase flow model, thus reducing the computational effort. To  
102 understand the potential limitations of the clustering approach, results from the semi-analytical  
103 multiphase flow model are compared with those obtained using a numerical model. Also, the  
104 influence of CO<sub>2</sub> leakage through existing abandoned wells located in the area of interest is  
105 studied.

106 The organization of this paper is as follows. First, the methodology of the study is  
107 described, which includes the multiphase flow semi-analytical algorithm, the generation of binary

108 permeability fields, and the statistical analysis. Then the application of the methodology to the  
109 Michigan Basin test site and results are presented. Lastly, a summary of conclusions is given.

## 110 **2 Methodology**

### 111 2.1 Multiphase Flow Semi-Analytical Model

112 ELSA-IGPS (Baù et al. 2015) is a multiphase flow simulator based upon the semi-  
113 analytical model ELSA developed by Celia and Nordbotten (2009) and Nordbotten et al. (2009).  
114 ELSA-IGPS is able to simulate the injection of supercritical CO<sub>2</sub> into a deep saline formation and  
115 compute the leakage of brine and CO<sub>2</sub> through poorly-sealed, “passive” wells. The domain is  
116 structured as a stack of horizontal, homogeneous, and isotropic aquifers separated by caprock  
117 layers, and perforated by a generic number of CO<sub>2</sub> injection wells and passive wells. CO<sub>2</sub> injection  
118 rates are assumed to be constant during the injection period, and no post-injection phase is  
119 simulated. Caprock layers are impermeable except at passive well locations. Initially, the domain  
120 is saturated with brine at hydrostatic pressure. Flow is assumed to be horizontal in aquifers and  
121 vertical in passive wells. Capillary pressure, dissolution and chemical reactions are neglected.  
122 The model considers a brine relative permeability equal to one in areas where no CO<sub>2</sub> is present,  
123 whereas in areas invaded by the CO<sub>2</sub> plume, the relative permeability of CO<sub>2</sub> is given by the end-  
124 point CO<sub>2</sub> relative permeability, which depends on the residual saturation of brine. The effective  
125 compressibility is assumed to be equal to the brine compressibility since most of the domain is  
126 filled with brine (Nordbotten et al. 2009). More details about the model assumptions can be found  
127 in Celia and Nordbotten (2009).

128 In ELSA (Nordbotten et al. 2005), fluid pressures changes are the compound effect of  
129 CO<sub>2</sub> injection and fluid leakage across caprock layers in passive wells. To determine the fluid  
130 overpressure, superposition of effects is applied based on a fundamental “well” function given in  
131 Celia et al. (2011). Using this approach, the fluid pressures  $p_{j,l}$  at the bottom of each aquifer  $l$   
132 ( $l=1,2,\dots,L$ ;  $L$  denotes the number of aquifers), at each passive well  $j$  ( $j=1,2,\dots,N$ ;  $N$  denotes the  
133 number of passive wells), and at any given time  $t$  are non-linear functions of the fluid densities,

134 viscosities, and compressibility, as well as the thickness, porosity, brine residual saturation and  
 135 permeability of the aquifers. These functions also depend on CO<sub>2</sub> injection rates entering aquifer  
 136  $l$  from each of the passive wells  $j$ . The cumulative fluid masses  $M_{j,l}(t)$  are calculated as

$$M_{j,l}(t) = \int_0^t \rho_{eff,j,l}(\tau) [Q_{j,l}(\tau) - Q_{j,l+1}(\tau)] d\tau, \quad (1)$$

137 where  $Q$  is the volumetric flow rate [ $L^3T^{-1}$ ] and  $\rho_{eff}$  is the effective fluid density [ $ML^{-3}$ ]. This  
 138 density is time-dependent since the composition of the leaking fluid varies upon the CO<sub>2</sub> plume  
 139 location. To calculate leakage rates  $Q_{j,l}$ , Nordbotten et al. (2005) propose to use the sum of the  
 140 flow rates  $Q_{\alpha,j,l}$  for each phase  $\alpha$  ( $b$  for brine and  $c$  for CO<sub>2</sub>) given by a multiphase version of  
 141 Darcy's law

$$Q_{j,l} = \sum_{\alpha=b,c} \left[ \pi r_{pw,j,l}^2 \frac{k_{r,\alpha,j,l} k_{pw,j,l}}{\mu_{\alpha} B_l} (p_{j,l-1} - \rho_{\alpha} g B_l - p_{j,l} - \rho_{\alpha} g H_{l-1}) \right]. \quad (2)$$

142 In Eq. (2),  $r_{pw}$  is the passive well radius [L],  $k_{pw}$  is the single-phase passive well permeability  
 143 [ $L^2$ ],  $\mu_{\alpha}$  is the dynamic viscosity of  $\alpha$  [ $ML^{-1}T^{-1}$ ],  $B$  is the aquitard thickness [L],  $p$  is the pressure  
 144 at the bottom of an aquifer [ $ML^{-1}T^{-2}$ ],  $g$  is the gravitational acceleration [ $LT^{-2}$ ] and  $H$  is the aquifer  
 145 thickness [L].

146 The substitution of Eqs. (1) and (2) in the expression of fluid pressures  $p_{j,l}$  leads to a  
 147 system of non-linear equations. In ELSA-IGPS (Baù et al. 2015), this system is efficiently solved  
 148 using a fixed-point scheme, which leads to a substantial computational saving when compared to  
 149 the linearization scheme adopted in ELSA by Nordbotten et al. (2005). Further details about the  
 150 model equations and solving procedures are given in Baù et al. (2015) and González-Nicolás et  
 151 al. (2015a).

## 152 2.2 Binary Permeability Fields

### 153 2.2.1 Generation of Binary Permeability Fields

154 Equally likely realizations of the caprock permeability spatial distribution are generated  
 155 with a categorical indicator Kriging simulator (CIKSIM), relying on a sequential Gaussian  
 156 simulation algorithm similar to that implemented in the “sgsim” routine available in the  
 157 Geostatistical Software Library (GSLIB) software developed by Deutsch and Journel (1998).

158 CIKSIM (González-Nicolás et al. 2015b) is based on a “multi-point” categorical geostatistics and  
159 has been developed to generate generic facies distributions characterized by arbitrary (continuous  
160 or discontinuous) and stationary local probability distribution functions (PDFs) and covariograms  
161 that may differ from category to category. CIKSIM approximates a generic cumulative  
162 probability distribution function (CDF) using a piecewise linear function. At any point in space  
163 during the simulation, the estimated conditional probabilities of the categories are used to  
164 randomly select the property values using the inverse CDF.

165 Note that other algorithms are available to generate caprock permeability field based on  
166 generic, non-Gaussian, CDFs such as those based on the normal score transform (Goovaerts 1997;  
167 Deutsch and Journel 1998) and Gaussian mixtures (Grana et al. 2012). For the purposes of this  
168 study, CIKSIM is used to create binary fields that include two types of facies (or categories).  
169 Facies 1 represents caprock areas with little or no permeability, and facies 2 represents inclusions  
170 characterized by a high permeability. Thus, CIKSIM generates inclusions of the caprock to  
171 introduce in the multiphase flow semi-analytical model explained in Sect. 2.1. The caprock  
172 permeability  $k$  is represented as a binary field (Deutsch and Journel 1998)

$$k(\mathbf{u}) = k_1 I(\mathbf{u}) + k_2 [1 - I(\mathbf{u})], \quad (3)$$

173 where  $k_1$  and  $k_2$  are the permeabilities of facies 1 and facies 2, respectively, at position  $\mathbf{u}$ , and  $I$   
174 is the indicator transform.

### 175 2.2.2 Clustering of Inclusions

176 If a large number of inclusions is generated for each field of the ensemble, the  
177 computational cost required by running the semi-analytical flow model (Sect. 2.1) will increase.  
178 To reduce this cost, a clustering algorithm of the inclusions is developed. A cluster is considered  
179 when two or more inclusion gridblocks are “in contact”, that is, when the distance between the  
180 centers of their gridblocks is less or equal to  $\sqrt{2} \cdot \Delta x$ , where  $\Delta x$  is the gridblock size adopted in  
181 the generation of the  $k$  field. The size and distribution of these clusters depend on the parameters  
182 assigned for their generation. In the semi-analytical model, each cluster is modeled as a single  
183 circular leakage spot (passive well) with an area equivalent to that of the cluster itself. The

184 position of the leakage spot is calculated as the centroid of the gridblocks forming the cluster.  
185 One example of grouping the clusters at the caprock is shown in Fig. 1. In this example, the  
186 number of 84 inclusions-blocks (orange gridblocks) is reduced to only 16 clusters after applying  
187 the clustering approach. The equivalent areas of the clusters are shown as black circles in Fig. 1.  
188 Each of these clusters is used as a single leaky point in the semi-analytical model ELSA-IGPS of  
189 Sect. 2.1.

190 [Figure 1 here]

191 Originally, ELSA-IGPS was developed to simulate multi-phase flow and estimate the  
192 leakage of both brine and CO<sub>2</sub> flux along existing passive wells. That is to say, leakage always  
193 occurs through small cross-sectional areas of the caprock (radii between 0.15 m – 1 m). In  
194 contrast, here, ELSA-IGPS is used to simulate escapes through larger weak areas of the caprock.  
195 A comparison with a numerical code is made to understand the limitations of using the semi-  
196 analytical model in this way. The comparison is carried out using the compositional version E300  
197 of ECLIPSE (Schlumberger 2010). ECLIPSE is a commercial numerical multi-phase flow model  
198 based on a three-dimensional finite-difference discretization and widely used in the gas and oil  
199 industry.

200 It is worth noting that the clustering approach is likely to alter the geostatistics of the  
201 inclusions and, in particular, their variogram. However, the most important requirement for this  
202 study is to maintain accuracy in the estimation of CO<sub>2</sub> leakage, as explained above, rather than  
203 preserving the geostatistics of the caprock.

### 204 2.3 Statistical Analysis

205 In this work, CO<sub>2</sub> leakage through caprock discontinuities and passive wells is quantified  
206 as the percentage of CO<sub>2</sub> mass,  $\%M_{leak}$ , released into aquifers overlying the targeted storage  
207 formation with respect to the total mass of CO<sub>2</sub> injected. CO<sub>2</sub> injection takes place in the deepest  
208 formation ( $l=1$ ) through a single injection well ( $M=1$ ), with only one overlying aquifer ( $l=2$ )  
209 above the injected aquifer considered (more details on the conceptual model are in Sect. 3.1).

210  $\%M_{leak}$  is calculated as the ratio between the mass of  $\text{CO}_2$  that escapes from the injected  
 211 formation into layer  $l=2$  and the total  $\text{CO}_2$  injected into layer  $l=1$  at final time  $t_{end}$

$$\%M_{leak} = \frac{M_{leak}(t_{end})}{\rho_c Q_{1,1} t_{end}} 100, \quad (4)$$

212 where  $M_{leak}(t_{end})$  is given by the net cumulative  $\text{CO}_2$  mass transferred into aquifer  $l=2$  through  
 213 all passive wells  $j$  ( $j=1,2,\dots,N$ )

$$M_{leak}(t_{end}) = \int_0^{t_{end}} [\sum_{j=1}^N \rho_c s_{c,j,2}(\tau) Q_{j,2}(\tau)] d\tau. \quad (5)$$

214 In Eq. (5)  $s_{c,j,2}$  represents saturation of  $\text{CO}_2$  at passive well  $j$  and aquifer  $l=2$ .

215 Output ensembles of the state variable  $\%M_{leak}$  are used to produce CDF plots. A CDF  
 216 of the state variable  $\%M_{leak}$  is obtained from the output of  $N_{MC}$  model simulations. After ordering  
 217 the  $\%M_{leak}$  values in ascending order,  $\%M_{leak_1} < \%M_{leak_2} < \dots < \%M_{leak_{N_{MC}}}$ , the  
 218 corresponding CDF values are calculated as  $CDF(\%M_{leak}) = (i - 0.5)/N_{MC}$  ( $i=1,2,\dots,N_{MC}$ )  
 219 (Hahn 1967). To optimize the performance of the simulations, preliminary tests are run to find  
 220 the minimum ensemble size  $N_{MC}$  beyond which CDFs remain substantially stationary. A sample  
 221 size of  $N_{MC} = 500$  is selected for each of the investigated scenarios.

222 The methodology applied in this study is summarized as follows. First, CIKSIM is  
 223 applied to the grid domain using conditional facies data, such as possible information on caprock  
 224 sealing properties in given areas. As a result, an ensemble of caprock binary fields containing the  
 225 two types of facies is obtained. The clustering approach is then applied to the caprock binary  
 226 fields in order to decrease the number of leaky areas to be introduced in the multiphase flow semi-  
 227 analytical model. After the completion of the clustering process, ELSA-IGPS Monte Carlo  
 228 simulations are run and a statistical analysis of the output ensembles of mass leakage are used to  
 229 generate CDF profiles. Figure 2 shows a flowchart of such methodology.

230 [Figure 2 here]

### 231 3 Application to the Michigan Basin Test Site

#### 232 3.1 Study Area

233 The methodology introduced in Sect. 2 is applied to a geological test site located within  
234 the Michigan Basin in proximity to the town of Thompsonville, MI. The candidate formation  
235 proposed for GCS is known as the Gray Niagaran formation. Fig. 3 shows a cross-section of the  
236 Michigan basin in the area of interest with the candidate storage formation highlighted in yellow.  
237 The Gray Niagaran formation lies below an almost depleted hydrocarbon reservoir (Brown  
238 Niagaran pinnacle in Fig. 3), which is currently used by Michigan Technological University for  
239 geophysical research.

240 [Figure 3 here]

241 The Gray Niagaran formation has a thickness of 119 m with its top at 1,500 m below the  
242 ground surface, making this formation appropriate as a geological repository of CO<sub>2</sub>. The choice  
243 to store supercritical CO<sub>2</sub> in this formation is justified by the sealing capacity of the formations  
244 above the Brown Niagaran pinnacle. However, a relevant source of uncertainty lies in the  
245 continuity of the caprock, highlighted in Fig. 3 (green shading). Although several data are  
246 available from monitoring wells at the test site (Halliburton 1990; SCH 1983, 1991), the  
247 information that can be used directly to describe the spatial distribution of the sealing properties  
248 of the caprock formation at the basin scale is scarce.

249 The model system is conceptualized in ELSA-IGPS as a stack of two aquifers ( $L=2$ ): the  
250 Gray Niagaran formation (119 m thick) below and the Carbonate formation (35 m thick) above.  
251 The two aquifers are separated by a 17-m thick caprock layer constituted by marine evaporites  
252 (Fig. 3). Supercritical CO<sub>2</sub> is injected into the Gray Niagaran formation through a single well.

253 When using the numerical simulator ECLIPSE, the geological model is also  
254 conceptualized as two aquifers separated by a caprock, with the same thicknesses described  
255 above. The model domain is divided into 100 m × 100 m gridblocks horizontally. Vertically, each  
256 formation is divided into four sub-layers. A single vertical CO<sub>2</sub> injection well is modeled at the  
257 center of the domain and screened within the lower aquifer. The grid resolution in the area

258 surrounding the injection well is progressively increased to achieve an appropriate size for a well  
 259 (about 0.5 m). To simulate a laterally infinite aquifer system, the pore volume of the boundary  
 260 gridblocks is multiplied by a factor of  $1 \times 10^6$ . In order to obtain comparable results with ELSA-  
 261 IGPS, the CO2SOL option of ECLIPSE is selected, which models the flow of two immiscible  
 262 fluids with no capillary pressure.

263 In both models, ELSA-IGPS and ECLIPSE, the mass injection rate is  $Q_m = 30$  kg/s (about  
 264 0.95 Mt/year) and remains constant during a simulated period of 10 years ( $t_{end}$  in Eq. (5)).  
 265 Initially, all formations are assumed to be saturated only with brine and under hydrostatic pressure  
 266 conditions. The caprock is assumed impermeable except for the location of inclusions or passive  
 267 wells located in the area of interest. A Van Genuchten constitutive model (Van Genuchten 1980)  
 268 is used to calculate relative permeabilities of CO<sub>2</sub> and brine, assuming a brine residual saturation  
 269  $s_b^{res} = 0.3$  and a fitting parameter of 0.41 (Zhou et al. 2009). Porosity values are extracted from the  
 270 log-wells of the two boreholes in Fig. 3 (Halliburton 1990; SCH 1983, 1991). The injected aquifer  
 271 and the overlying formation are assumed to have a permeability equal to  $2.8 \times 10^{-14}$  m<sup>2</sup> and  $9.6 \times 10^{-15}$   
 272 m<sup>2</sup>, respectively, calculated according to Trebin (1945) as

$$\begin{aligned}
 k &= 2e^{31.6\varphi} && \text{if } 100\varphi < 12\% \\
 k &= 4.94(100\varphi)^2 - 763 && \text{if } 100\varphi > 12\% \quad , \quad (6)
 \end{aligned}$$

273 where:  $k$  is the permeability in millidarcy (mD,  $1\text{mD} \equiv 1 \times 10^{-15}$  m<sup>2</sup>), and  $\varphi$  is the porosity ( $l$ ). For  
 274 the comparison of ELSA-GPS and ECLIPSE results, the sealing formation is assigned a  
 275 permeability  $k_1 = 0$ . For simplicity, inclusions in the caprock are assumed to have the same  
 276 permeability as the injected aquifer  $l=1$  ( $k_2 = k_{l_1}$ ). The hydro-geomechanical parameters used in  
 277 this study are provided in Table 1.

278 [Table 1 here]

### 279 3.2 Caprock Permeability Generation

280 In order to generate caprock permeability realizations, CIKSIM is used. For this purpose,  
 281 a grid covering an area of 7 km  $\times$  7 km is considered with the hydrocarbon reservoir located at its  
 282 center (Fig. 1). Each gridblock is 100 m  $\times$  100 m, yielding a total of 4,900 blocks. The thickness

283 of the caprock above the Gray Niagaran formation is relatively small when compared to the  
 284 horizontal extension of this formation (30.5 m thickness of caprock versus 7,000 m of estimated  
 285 grid extension), thus the permeability is represented as a two-dimensional heterogeneous field  
 286 with no variation in the vertical direction.

287 Since the reservoir has contained oil before, it is assumed that the caprock in its area is  
 288 perfectly impermeable. This information is used to “condition” caprock permeability realizations  
 289 as facies 1 in the gridblocks inside the reservoir boundary. The caprock permeability in the other  
 290 gridblocks (unsampled locations) is unknown and thus simulated stochastically. In Fig. 1, the  
 291 lateral boundary of the reservoir is indicated by the blue line, and red dots correspond to  
 292 gridblocks where the permeability is that of facies 1.

### 293 3.2.1 Uncertainty from Caprock Continuity

294 The generation of the caprock permeability ensembles with CIKSIM is based on the two-  
 295 point geostatistics described in Table 2. The following exponential covariance model is used for  
 296 both facies

$$C_{k_i k_i}(d; \sigma_{k_i}^2, l_{k_i}) = \sigma_{k_i}^2 \exp\left(-\frac{d}{l_{k_i}}\right) \quad (i = 1, 2), \quad (7)$$

297 where:  $d$  is the horizontal distance between any two points;  $\sigma_{k_1}^2, \sigma_{k_2}^2$ , and  $l_{k_1}, l_{k_2}$  are the variances  
 298 and the correlation lengths of the two facies; and  $k_1$  and  $k_2$  are the permeability of facies 1 and  
 299 2, respectively. Note that  $\sigma_{k_1}^2 = P_1(1 - P_1)$  and  $\sigma_{k_2}^2 = P_2(1 - P_2)$ , where  $P_1$  and  $P_2$  are the  
 300 probability of facies 1 and 2, respectively. Several probabilities of the occurrence of  $P_2$  are applied  
 301 for facies 2 (inclusions) ranging between 0.0005 and 0.02, as well as correlation lengths  $l_{k_2} = l_{xy}$   
 302 ranging between 200 m and 1,500 m ( $xy$  denotes equal correlation lengths in the  $x$  and  $y$   
 303 directions. Facies 1 has a probability  $P_1 = 1 - P_2$ , and a correlation length  $l_{k_1} = 1,000$  m in all  
 304 scenarios.  $N_{MC}$  in Table 2 refers to the ensemble size.

305 [Table 2 here]

306 To analyze the caprock permeability field generated by CIKSIM in relation to the  
 307 correlation length  $l_{xy}$  and the effect that this has on CO<sub>2</sub> leakage, two parameters are here

308 introduced: the average distance  $D$  between the inclusion clusters and the injection well; and the  
 309 inclusion ratio  $r_{lc}$ . The distance  $D$  is calculated as

$$D = \frac{1}{N_{MC}} \sum_{j=1}^{N_{MC}} \frac{\sum_{i=1}^{N_{cl}} d_{i,j}}{N_{cl}}, \quad (8)$$

310 where  $N_{cl}$  ( $i=1,2,\dots, N_{cl}$ ) is the total number of clusters present in realization  $j$  ( $j=1,2,\dots, N_{MC}$ ), and  
 311  $d_{i,j}$  is the distance between the center of the cluster  $i$  in realization  $j$  and the injection well. In  
 312 general, one can expect CO<sub>2</sub> leakage to be probabilistically more pronounced for smaller values  
 313 of  $D$ , which practically indicates how close to the injection well the inclusions are on average.

314 The inclusion ratio  $r_{lc}$  is defined as the fraction between the average number of actual  
 315 inclusion blocks generated in the ensemble and the expected number of inclusion blocks

$$r_{lc} = \frac{\frac{\sum_{j=1}^{N_{MC}} l_{c,j}}{N_{MC}}}{P_2 N_{gb}}, \quad (9)$$

316 where  $N_{gb}$  is the total number of gridblocks considered for the generation of the caprock ( $N_{gb}=$   
 317 4,900), and  $l_{c,j}$  is the number of inclusion gridblocks in realization  $j$ . For instance, for a  
 318 probability  $P_2 = 0.01$ , the expected number of inclusion blocks is 49 ( $P_2 N_{gb}$ ). In general, larger  
 319  $r_{lc}$  values indicate the presence of larger inclusions than expected, which should probabilistically  
 320 produce larger CO<sub>2</sub> leakage.

321 Finally, to investigate the influence of the injected formation permeability and inclusions  
 322 permeability on CO<sub>2</sub> leakage, different combinations of these are considered as in the scenarios  
 323 1.1, 2.1, 3.1, 4.1, and 5.1 presented in Table 2. The range of permeabilities of the injected  
 324 formation  $k_{l_1}$  and inclusions  $k_2$  studied spans from  $1 \times 10^{-15}$  m<sup>2</sup> (about 1 mD) to  $1 \times 10^{-12}$  m<sup>2</sup> (about  
 325 1,000 mD). Results of these analyses are reported in terms of the 95<sup>th</sup> percentile of  $\%M_{leak}$  (Eq.  
 326 (4)).

### 327 3.2.2 Uncertainty from Caprock Continuity and Passive Wells Permeability

328 The study area considered in Sect. 3.1 comprises 60 wells that perforate the candidate  
 329 formation to store CO<sub>2</sub>. The locations of these wells are obtained from the Michigan Department  
 330 of Environmental Quality database (MDEQOGD 2014). The integrity of these wells is uncertain.

331 A deteriorated or poorly cemented well can create a leaky pathway for brine and/or CO<sub>2</sub>. Since  
332 the number of these passive wells is significant, they are included in the uncertainty analysis for  
333 CO<sub>2</sub> leakage.

334 Before use in the semi-analytical model, these 60 passive wells are grouped into 20  
335 equivalent leaky pathways following the approach outlined in González-Nicolás et al. (2015a).  
336 Following this approach, these groups are identified by minimizing the sum of the Euclidean  
337 distances of the passive wells that form a cluster of wells and the cluster centroid. The equivalent  
338 leaky area considered for each cluster of wells is equal to the sum of the cross-sectional areas of  
339 the wells included in that group. From the equivalent leaky area, an equivalent radius is calculated  
340 and introduced into Eq. (2) to compute the flow rate through this cluster. Figure 4 shows the  
341 positions of the 60 passive wells and the position of the 20 equivalent groups of wells after  
342 clustering.

343 [Figure 4 here]

344 The location of these well groups is fixed in each of the realizations of the caprock  
345 permeability, but their permeability is considered stochastic, as no information is available on  
346 passive well integrity. All passive well permeabilities are assumed to fit to the same lognormal  
347 probability distribution function with a log-mean of  $\log(1 \times 10^{-14} \text{ m}^2)$  and a log-standard deviation  
348 of 1 log-m<sup>2</sup> (Nordbotten et al. 2009).

## 349 **4 Results and Discussion**

### 350 **4.1 Simulating CO<sub>2</sub> Leakage from Large Caprock Areas Using ELSA-IGPS**

351 To investigate the viability of simulating CO<sub>2</sub> leakage across generic caprock inclusions  
352 with the semi-analytical model, results of ELSA-IGPS are compared with those of the numerical  
353 model ECLIPSE. Results of the comparison are summarized in Fig. 5 and Fig. 6.

354 Figure 5 presents the cumulative mass leakage of CO<sub>2</sub> over time for two representative  
355 caprock permeability realizations from scenario 3.1. These two realizations are shown in Fig. 5a  
356 and 5b, whereas the corresponding CO<sub>2</sub> leakage profiles are shown in Fig. 5c and 5d. In both

357 realizations, the final (at  $t_{end} = 10$  years) cumulative CO<sub>2</sub> mass leakage given by ELSA-IGPS  
358 and that given by ECLIPSE are quite similar. In addition, the final cumulative CO<sub>2</sub> mass leakages  
359 in the two realizations are of the same order of magnitude. However, for the realization in Fig.  
360 5a, the CO<sub>2</sub> mass leakage simulated by ECLIPSE starts earlier than that obtained with ELSA-  
361 IGPS (Fig. 5c). These differences are not observed in Fig. 5d, which relates to the realization  
362 shown in Fig. 5b.

363 [Figure 5 here]

364 The analysis of the two models' results for several other realizations of the caprock  
365 permeability (results not shown here) suggests that ECLIPSE simulates consistently an earlier  
366 CO<sub>2</sub> leakage than ELSA-IGPS's when caprock discontinuities are located farther away from the  
367 CO<sub>2</sub> injection well. In this respect, a major difference between the realizations in Figs. 5a and 5b  
368 lies in the distance at which the closest inclusion to the CO<sub>2</sub> injection well is found. In Fig. 5a  
369 such distance is 1,532 m, whereas in Fig. 5b it is 526 m. Numerical tests conducted in this study  
370 show that this distance is a crucial parameter for the comparison, and discrepancies between the  
371 two models, in terms of CO<sub>2</sub> leakage versus time, are observed only when this minimum distance  
372 is greater than about 600 m (Figs. 4a and 4c). For realizations having the closest inclusion within  
373 600 m (Fig. 5b) no substantial difference in the CO<sub>2</sub> mass leakage profiles is found (Fig. 5d).

374 The earlier CO<sub>2</sub> leakage simulated by ECLIPSE as compared to ELSA-IGPS has already  
375 been observed by Nordbotten et al. (2009), who attributed these differences to numerical diffusion  
376 in ECLIPSE. Our results confirm these observations. Effects of numerical diffusion lead to  
377 simulating a more spread out CO<sub>2</sub> plume front at any given time, that is, a CO<sub>2</sub> plume that  
378 somehow advances faster. This results in an earlier leakage, particularly when inclusions are  
379 located farther away from the injection well, since in this case the CO<sub>2</sub> plume has to travel longer  
380 distances before leakage starts, exacerbating the effects of numerical diffusion.

381 Figure 6 shows the CDF of  $\%M_{leak}$  (Eq. (4)) of ELSA-IGPS (in red) and ECLIPSE (in  
382 blue) for scenarios 2.1 (dashed lines) and scenario 4.1 (solid lines). One can observe that CO<sub>2</sub>  
383 mass leakage for the two codes is quite similar for  $\%M_{leak}$  values greater than 1%, whereas larger

384 discrepancies are found for smaller  $\%M_{leak}$  values. Also, differences in  $\text{CO}_2$  leakage are more  
385 pronounced for larger inclusion probabilities  $P_2$ . Statistically, ECLIPSE produces more leakage  
386 of  $\text{CO}_2$  than ELSA-IGPS, which can also be explained by the effects of numerical diffusion  
387 discussed above. The analysis of the CDFs in Fig. 6 reveals that low ranges of  $\%M_{leak}$  are  
388 characterized by realizations with inclusions located farther away from the injection well, in  
389 which the  $\text{CO}_2$  leakage simulated by ELSA-IGPS starts later than ECLIPSE's, thus producing a  
390 lower  $\%M_{leak}$ .

391 [Figure 6 here]

392 In general, the cumulative  $\text{CO}_2$  mass leakage produced by the two models is of the same  
393 order of magnitude at later times, hence showing a reasonably good agreement between the two  
394 approaches. But since the computational cost of ELSA-IGPS is about two/three orders of  
395 magnitude lower than ECLIPSE's, the advantage achieved by introducing clustered inclusions  
396 into ELSA-IGPS is quite significant for quantifying the uncertainty on  $\text{CO}_2$  leakage at the  
397 considered site.

## 398 4.2 Quantifying Uncertainty on Caprock Continuity

### 399 4.2.1 Testing of Binary Permeability Fields

400 Figure 7 shows profiles of the average distance  $D$  (Eq. (8)) and the inclusion ratio  $r_{lc}$  (Eq.  
401 (9)) as functions of the correlation length  $l_{xy}$ . In Fig. 7a, the  $D$  versus  $l_{xy}$  relationship is graphed  
402 for probabilities  $P_2$  equal to 0.005, 0.01, and 0.02. In general, as the correlation length  $l_{xy}$  of  
403 facies 2 increases, the distance  $D$  is observed to decrease at first and then become roughly  
404 constant. In practice, low correlation lengths lead to generating smaller inclusions, generally  
405 spread out throughout the domain and thus situated – on average – farther away from the injection  
406 well. On the other hand, larger correlation lengths signify larger inclusions, which are constrained  
407 within the domain and thus lead to smaller values of  $D$ . As a result, for a given probability  $P_2$  and  
408 different correlation lengths, larger  $l_{xy}$  values will reflect larger  $\text{CO}_2$  mass leakage because the

409 average distance  $D$  that the  $\text{CO}_2$  plume has to travel through the storage formation to reach  
410 caprock inclusions, and thus the travel time, will be shorter.

411 [Figure 7 here]

412 Figure 7b displays the relationship between correlation length  $l_{xy}$  and the inclusion ratio  
413  $r_{lc}$  for probabilities  $P_2$  equal to 0.005, 0.01, and 0.02. This figure shows that in general  $r_{lc}$  is equal  
414 to 1 only when the correlation length is very small ( $l_{xy}= 0.1$  m) and exhibits a general increasing  
415 trend as  $l_{xy}$  increases. This trend is, however, not significant for correlation lengths  $l_{xy}$  beyond  
416 400 m, where  $r_{lc}$  becomes roughly constant with values oscillating between 1.6 and 1.8 depending  
417 on the assigned probability  $P_2$ . This indicates that, in order to simulate caprock continuity and its  
418 impact on the uncertainty on  $\text{CO}_2$  leakage, assigning meaningful values of the correlation  $l_{xy}$  can  
419 be as significant as assessing the inclusion probability  $P_2$ .

#### 420 4.2.2 Quantifying $\text{CO}_2$ Leakage

421 The effects of the correlation length  $l_{xy}$  and the inclusion probability of facies 2 on  $\text{CO}_2$   
422 leakage are summarized in Fig. 8, which shows the CDF of  $\%M_{leak}$  (Eq. (4)) for some of the  
423 scenarios described in Table 2. In general,  $\text{CO}_2$  mass leakage is higher for larger  $P_2$  values. This  
424 is not surprising, since a higher  $P_2$  substantially means a higher probability of the  $\text{CO}_2$  plume to  
425 encounter leakage pathways across the caprock. It is interesting to observe, however, that if a  
426 maximum  $\%M_{leak}$  target of  $1 \times 10^{-3}$  is prescribed, this is met with an 81% probability in scenario  
427 1.1 ( $P_2= 0.0005$  and  $l_{xy}= 200$  m) and only with a 1% probability in scenario 5.1 ( $P_2= 0.02$  and  
428  $l_{xy}= 200$  m).

429 [Figure 8 here]

430 Results in Fig. 7 confirm that the  $\%M_{leak}$  associated to caprock permeability fields with  
431 the same probability  $P_2$  is larger for larger correlation lengths, since inclusions have larger extent  
432 and, consequently, the  $\text{CO}_2$  mass leakage is more likely to occur. This is in agreement with two  
433 points made previously: i) the distance from the center cluster to the injection well  $D$  is lower for

434 a higher correlation length (Fig. 7a); and ii) the inclusion ratio is greater for higher correlation  
435 lengths (Fig. 7b). For example, there are, on average, more inclusions in a scenario where  $l_{xy} =$   
436 1,500 m, than when  $l_{xy} = 200$  m, and the distance that the CO<sub>2</sub> plume has to travel to reach the  
437 center of inclusion clusters is shorter, thus promoting earlier leakage of CO<sub>2</sub>.

#### 438 4.2.3 Influence of Permeability Values of the Injected Formation and Inclusions

439 To study the combined influence of the storage formation permeability  $k_{l_1}$  and the  
440 inclusions permeability  $k_2$  on the maximum probable amount of leaked CO<sub>2</sub>, different  
441 combinations of  $k_{l_1}$  and  $k_2$  are considered for scenarios 1.1, 2.1, 3.1, 4.1, and 5.1 (Table 2). These  
442 results are presented in Fig. 9, which shows contour maps of the % $M_{leak}$  95<sup>th</sup> percentile as a  
443 function of  $k_{l_1}$  and  $k_2$ . Each subpanel in Fig. 9 corresponds to one of the scenarios above. All  
444 scenarios exhibit the lowest CO<sub>2</sub> mass leakage when  $k_{l_1}$  is high and  $k_2$  is low. In general, high  
445 permeability of the injection formation *corresponds* to less escape of CO<sub>2</sub> through weak areas.  
446 The CO<sub>2</sub> plume advances more easily through the injected formation when  $k_{l_1}$  is high, which  
447 enhances its injectivity and storage properties, and limits CO<sub>2</sub> escape, particularly if the inclusion  
448 permeability  $k_2$  is low. As indicated in Fig. 9, scenarios 1.1 and 2.1 are those characterized by  
449 the lowest CO<sub>2</sub> mass leakages. In scenarios 4.1 (Fig. 9d) and 5.1 (Fig. 9e), considerable amounts  
450 of CO<sub>2</sub> leakage are observed when the inclusion permeability is greater than  $3.16 \times 10^{-13} \text{ m}^2$   
451 ( $\log k_2 = -12.5$ ). Broadly, results of these scenarios show that % $M_{leak}$  is more sensitive to  $k_{l_1}$   
452 than  $k_2$ , except when permeability of inclusions presents a very high value of  $k_2$  ( $\log k_2 \geq -12.5$ ).  
453 These results are aligned with those in González-Nicolás et al. (2015a), which have shown that  
454 the permeability of the storage formation has the greatest impact on CO<sub>2</sub> leakage uncertainty,  
455 whereas the permeability of passive wells, which can be seen as analogues for inclusions, has a  
456 significant influence on CO<sub>2</sub> leakage through the interaction with other parameters (higher order  
457 effects), such as the location of the leaky pathways.

458 [Figure 9 here]

459 The  $\%M_{leak}$  maps given Fig. 9 can be used in relation to the metric reported by Pacala  
460 (2003), which limits the amount of CO<sub>2</sub> leakage returning to the atmosphere to 1% per one year.  
461 In scenario 1.1 (Fig. 9a), where the probability of finding an inclusion is the lowest,  $\%M_{leak}$   
462 would be less than or equal to 1% per one year for values of  $k_{l_1}$  greater than  $5.01 \times 10^{-14} \text{ m}^2$   
463 ( $\log k_{l_1} \geq -13.3$ ). On the other hand, if  $P_2$  is increased to 0.01 (Fig. 9d), in order to maintain the  
464 maximum probable CO<sub>2</sub> leakage below the 1% per year threshold, the minimum permeability  
465 required for the injection formation and the inclusions should be  $3.98 \times 10^{-13} \text{ m}^2$  ( $\log k_{l_1} = -12.4$ )  
466 and  $6.31 \times 10^{-14} \text{ m}^2$  ( $\log k_{l_2} = -13.2$ ), respectively.

467 This analysis shows that geostatistical data, such as the probability  $P_2$  and the correlation  
468 length,  $l_{xy}$ , play a critical role for the probabilistic assessment of CO<sub>2</sub> leakage prior to the GCS  
469 development for a candidate reservoir. For instance, Fig. 9 indicates that a probability  $P_2$  greater  
470 than 0.001 with  $l_{xy} = 200 \text{ m}$  (scenarios 2.1, 3.1, 4.1, and 5.1) is likely to produce a CO<sub>2</sub> leakage  
471 greater than 1% per year, in which case the injections of CO<sub>2</sub> into the candidate storage formation  
472 should not be recommended. If the permeability of the storage formation is  $k_{l_1} = 2.8 \times 10^{-14} \text{ m}^2$   
473 ( $\log k_{l_1} = -13.55$ ) (Table 1), injection of CO<sub>2</sub> into the formation is not viable since this would lead  
474 to a probability of CO<sub>2</sub> leakage exceeding 1% independently of the  $P_2$  value considered in the  
475 scenarios shown in Fig. 9. It is, however, important to emphasize that these estimates are quite  
476 conservative since the limit proposed by Pacala (2003) is on CO<sub>2</sub> leakage rates back to the  
477 atmosphere, whereas in this study the CO<sub>2</sub> mass leakage considered is the CO<sub>2</sub> that escapes the  
478 target storage formation  $l=1$ . Additional processes of trapping and attenuation that CO<sub>2</sub> may  
479 undergo in the overburden formations are not accounted for.

#### 480 4.3 Combining the Effects of Caprock Inclusions and Passive Wells

481 Uncertainty from permeability of passive wells affects CO<sub>2</sub> mass leakage results when  
482 this uncertainty is added to caprock continuity uncertainty, especially in scenarios where CO<sub>2</sub>  
483 leakage from the caprock discontinuities is expected to be low. Figure 10 and Fig. 11 show CDFs  
484 of  $\%M_{leak}$  (Eq. (4)) for some of the scenarios described in Table 2 in the cases where uncertainty

485 in passive well is (solid lines) and is not (dashed lines) accounted for. In Fig. 10, the selected  
486 inclusion scenarios are those characterized by the same correlation length  $l_{xy}=200$  m (scenarios  
487 2.1, 3.1, 4.1, and 5.1). Results in Fig. 10 reveal that, for the considered test site, uncertainty from  
488 permeability of passive wells does not affect significantly CO<sub>2</sub> mass leakage, independently of  
489 the prescribed  $P_2$  value, if  $\%M_{leak}$  exceeds 1%; yet significant differences are observed for  
490 smaller values of  $\%M_{leak}$ , especially for the lowest probabilities  $P_2$  of the inclusions (e.g.,  $P_2=$   
491 0.0005 and  $P_2=0.001$ ).

492 [Figure 10 here]

493 In Fig. 10, scenario 1.1 (blue lines), which has the lowest inclusion probability  $P_2$ , shows  
494 an 82% probability of  $\%M_{leak}$  to be less than  $1\times 10^{-3}$  when only caprock continuity uncertainty is  
495 considered (blue dashed line). When adding the uncertainty from passive well permeability (blue  
496 solid line) this probability is reduced to zero, and there is practical certainty to exceed the  $1\times 10^{-3}$   
497 threshold. Scenarios 2.1, 3.1, and 4.1 exhibit the same tendency as in scenario 1.1. However,  
498 scenarios with higher probability  $P_2$ , such as scenario 4.1 (green profile) and 5.1 (in gray), show  
499 small differences between their CDFs even for low values of  $\%M_{leak}$ . Moreover, in scenario 5.1  
500 (gray profile) the influence on leakage produced by the uncertainty on the permeability of passive  
501 wells is negligible in comparison to the leakage produced through the weak areas of the caprock.

502 Similar to Fig. 10, Fig. 11 shows CDFs of  $\%M_{leak}$  (Eq. (4)) for scenarios 2.1, 2.2, 2.3  
503 and 2.4 in Table 2, characterized by the same probability  $P_2$  and different correlation lengths,  
504 when uncertainty in passive wells is (solid lines) and is not (dashed lines) considered. Results of  
505 Fig. 11 indicate that uncertainty on passive wells permeability has an important impact on the  
506 CDFs for values of  $\%M_{leak}$  below 0.25%, independently of the correlation length. Figure 11 also  
507 shows that when uncertainty on passive wells is considered, the influence of the inclusion  
508 correlation scale  $l_{xy}$ , which practically dictates the size of the inclusions, is noticeable for  
509  $\%M_{leak}$  equal to 0.1% and becomes more prominent for  $\%M_{leak}$  larger than 1%. On the other

510 hand, when uncertainty on passive wells is not considered, the influence of  $l_{xy}$  is noticed at much  
511 lower leakage values ( $\%M_{leak} = 1 \times 10^{-3}\%$ ).

512 [Figure 11 here]

## 513 **5 Summary and Conclusions**

514 This work advances a novel methodology for the preliminary assessment of the suitability  
515 of saline aquifers for GCS in relation to the risk of CO<sub>2</sub> leakage across high permeable areas of  
516 the caprock. The study is focused on inclusion facies but it also considers the presence of  
517 passive/abandoned wells of uncertain integrity. This framework is applied to a saline aquifer  
518 embedded within the Michigan sedimentary basin, with very limited information on the sealing  
519 properties of the caprock. An uncertainty quantification analysis of CO<sub>2</sub> leakage is conducted by  
520 developing a Monte Carlo simulation approach, where the caprock permeability field is the major  
521 source of uncertainty. Because of the computational cost involved in the use of numerical  
522 multiphase flow numerical models, the viability of substituting them with a semi-analytical flow  
523 model originally developed to treat leakage from passive wells is studied. To generate caprock  
524 discontinuities a two-point geostatistics simulator of permeability is coupled with a clustering  
525 algorithm that produces equivalent circular discontinuities for direct use in the semi-analytical  
526 flow model. To understand the limitations of applying the semi-analytical model to simulate  
527 leakage through large areas of the caprock, a comparison of the semi-analytical algorithm with a  
528 numerical code is carried out. Results show that, in general, there is a good agreement between  
529 the two models, with the cumulative CO<sub>2</sub> mass leakage produced being practically the same at  
530 later times.

531 Parameters such as  $D$  and  $r_{lc}$  can be regarded as useful indicators for assessing the  
532 vulnerability of any site to CO<sub>2</sub> leakage. Since CO<sub>2</sub> leakage varies greatly depending on  $P_2$  and  
533  $l_{xy}$  values, it is critical to prescribe realistic values of  $P_2$  and  $l_{xy}$  to be able to quantify uncertainty  
534 in CO<sub>2</sub>. Uncertainty from passive well permeability has less impact on CO<sub>2</sub> leakage when large

535 amounts of CO<sub>2</sub> leakage through the inclusions are expected ( $\%M_{leak} > 1\%$ ) and is only  
536 significant when CO<sub>2</sub> leakages from caprock inclusions are low.

537 Overall, seemingly low inclusion probabilities  $P_2$ , of the order of 1%, may lead to  
538 considerable CO<sub>2</sub> leakage. Therefore, extreme caution should be used before injection of CO<sub>2</sub> into  
539 the selected candidate formation. While processes of trapping and attenuation that CO<sub>2</sub> may  
540 undergo in the overburden formations are expected, to enhance GCS safety, only the collection  
541 of high resolution geophysical data over a large area around the injection site may help narrow  
542 down the uncertainty on the caprock continuity.

543 Finally, the methodology presented here can be transferred to assess the probability and  
544 intensity of CO<sub>2</sub> leakage in other potential GCS candidate sites in which data on the caprock  
545 sealing properties are limited or inexistent. Since this situation is often encountered in the real  
546 world, this framework can offer a valid tool to support decision makers in the preliminary  
547 selection of safe GCS sites.

## 548 **6 Acknowledgements**

549 This research was supported by the U. S. Department of Energy, National Energy  
550 Technology Laboratory (DOE Project: DE-FE0001830). The research conducted was also made  
551 possible with the support of Schlumberger Ltd., who kindly donated the reservoir simulation  
552 software suites PETREL and ECLIPSE. The research team is also grateful to Michigan  
553 Technological University's Professor Roger Turpening for providing access to the data library  
554 regarding the Niagara formations to which this research has been applied, as well as continued  
555 support to the use of this library.

## 556 **7 References**

557 Bachu S (2003) Screening and ranking of sedimentary basins for sequestration of CO<sub>2</sub> in  
558 geological media in response to climate change. *Environ Geol* 44(3):277-289.  
559 doi:10.1007/s00254-003-0762-9

560 Baù D, Cody B, González-Nicolás A (2015) An iterative global pressure solution for the semi-  
561 analytical simulation of geological carbon sequestration. *Computat Geosci* 19(4):781-  
562 789. doi:10.1007/s10596-015-9489-4

563 Bergman PD, Winter EM (1995) Disposal of carbon-dioxide in aquifers in the US. *Energ Convers*  
564 *Manage* 36(6-9):523-526. doi:10.1016/0196-8904(95)00058-1

565 Celia MA, Nordbotten JM (2009) Practical modeling approaches for geological storage of carbon  
566 dioxide. *Ground Water* 47(5):627-638. doi:10.1111/j.1745-6584.2009.00590.x

567 Celia MA, Nordbotten JM, Court B, Dobossy M, Bachu S (2011) Field-scale application of a  
568 semi-analytical model for estimation of CO<sub>2</sub> and brine leakage along old wells. *Int J*  
569 *Greenh Gas Con* 5(2):257-269. doi:10.1016/j.ijggc.2010.10.005

570 Celia MA, Bachu S, Nordbotten JM, Bandilla K (2015) Status of CO<sub>2</sub> storage in deep saline  
571 aquifers with emphasis on modeling approaches and practical simulations. *Water Resour*  
572 *Res* 51(9):6846-6892. doi:10.1002/2015WR017609

573 Chang KW, Minkoff S, Bryant S (2008) Modeling leakage through faults of CO<sub>2</sub> stored in an  
574 aquifer. SPE Annual Technical Conference and Exhibition. Society of Petroleum  
575 Engineers. doi:10.2118/115929-ms

576 Deutsch CV, Journel AG (1998) *GSLIB: geostatistical software library and user's guide*. New  
577 York : Oxford University Press, Version 2.0, 2nd ed.

578 Gasda SE, Bachu S, Celia MA (2004) Spatial characterization of the location of potentially leaky  
579 wells penetrating a deep saline aquifer in a mature sedimentary basin. *Environ Geol* 46(6-  
580 7):707-720. doi:10.1007/s00254-004-1073-5

581 González-Nicolás A, Baù D, Cody BM, Alzraiee A (2015a) Stochastic and global sensitivity  
582 analyses of uncertain parameters affecting the safety of geological carbon storage in  
583 saline aquifers of the Michigan Basin. *Int J Greenh Gas Con* 37:99-114.  
584 doi:10.1016/j.ijggc.2015.03.008

585 González-Nicolás A, Baù D, Alzraiee A (2015b) Detection of potential leakage pathways from  
586 geological carbon storage by fluid pressure data assimilation. *Adv Water Resour* 86:366-  
587 384. doi:10.1016/j.advwatres.2015.10.006

588 Goovaerts P (1997) Geostatistics for natural resources evaluation. Applied Geostatistics Series,  
589 Oxford University Press on Demand, New York

590 Grana D, Mukerji T, Dovera L, Della Rossa E (2012) Sequential simulations of mixed discrete-  
591 continuous properties: Sequential Gaussian mixture simulation, Geostatistics Oslo 2012.  
592 Springer, pp. 239-250

593 Hahn GJ (1967) Statistical models in engineering. Wiley series on systems engineering and  
594 analysis. Wiley, New York

595 Halliburton (1990) Log 21101375660000 Stech Upper Half (Date: 09/04/1990)

596 International Energy Agency (2008) Carbon capture and storage: meeting the challenge of climate  
597 change. IEA/OECD. Paris

598 Journel AG, Alabert F (1989) Non-Gaussian data expansion in the Earth sciences. Terra Nova 1  
599 (2):123-134. doi:10.1111/j.1365-3121.1989.tb00344.x

600 Kopp A, Binning PJ, Johannsen K, Helmig R, Class H (2010) A contribution to risk analysis for  
601 leakage through abandoned wells in geological CO<sub>2</sub> storage. Adv Water Resour  
602 33(8):867-879. doi:10.1016/j.advwatres.2010.05.001

603 Krige DG (1951) A statistical approach to some mine valuations and allied problems on the  
604 Witwatersrand. M.Sc. Eng. Thesis of University of Witwatersrand, Johannesburg

605 MDEQOGD (2014) Michigan Department of Environmental Quality Oil and Gas Database,  
606 [http://www.michigan.gov/deq/0,4561,7-135-6132\\_6828-98518--,00.html](http://www.michigan.gov/deq/0,4561,7-135-6132_6828-98518--,00.html). Accessed  
607 03/08/2014. [http://www.michigan.gov/deq/0,4561,7-135-6132\\_6828-98518--,00.html](http://www.michigan.gov/deq/0,4561,7-135-6132_6828-98518--,00.html)

608 Metz B, Intergovernmental Panel on Climate Change. Working Group III. (2005) IPCC Special  
609 report on carbon dioxide capture and storage. Cambridge University Press, for the  
610 Intergovernmental Panel on Climate Change, Cambridge

611 Nicholls N, Gruza G, Jouzel J, Karl T, Ogallo L, Parker D (1996) Observed climate variability  
612 and change. Cambridge University Press

613 Nogues JP, Court B, Dobossy M, Nordbotten JM, Celia MA (2012) A methodology to estimate  
614 maximum probable leakage along old wells in a geological sequestration operation. Int J  
615 Greenh Gas Con 7:39-47. doi:10.1016/j.ijggc.2011.12.003

616 Nordbotten JM, Celia MA, Bachu S, Dahle HK (2005) Semianalytical solution for CO<sub>2</sub> leakage  
617 through an abandoned well. *Environ Sci Technol* 39(2):602-611. doi: 10.1021/es035338i

618 Nordbotten JM, Kavetski D, Celia MA, Bachu S (2009) Model for CO<sub>2</sub> leakage including multiple  
619 geological layers and multiple leaky wells. *Environ Sci Technol* 43(3):743-749. doi:Doi  
620 10.1021/Es801135v

621 Pacala SW (2003) Global constraints on reservoir leakage. In: Gale J, Kaya Y (eds) *Greenhouse*  
622 *Gas Control Technologies – 6<sup>th</sup> International Conference*. Pergamon, Oxford, pp 267-  
623 272. doi:http://dx.doi.org/10.1016/B978-008044276-1/50043-X

624 Ruether JA (1998) FETC Programs for reducing greenhouse gas emissions. (No. DOE/FETC-  
625 98/1058). USDOE Federal Energy Technology Center, Pittsburgh, PA (United States)

626 Sakamoto Y, Tanaka A, Tenma N, Komai T (2011) Numerical study on flow behavior of CO<sub>2</sub> in  
627 an aquifer for risk assessment of carbon capture and storage. *Energy Procedia* 4:4170-  
628 4177. doi:10.1016/j.egypro.2011.02.363

629 SCH (1983) Log 21101365880000 Burch Main Suite (Date 06/19/1983)

630 SCH (1991) Log 21101375660000 Stech Lower Half (Date: 06/29/1991)

631 Schlumberger (2010) Eclipse technical description, v. 2010.1, Report, Abingdon, U.K.

632 Solomon S, Intergovernmental Panel on Climate Change., Intergovernmental Panel on Climate  
633 Change. Working Group I. (2007) *Climate change 2007: the physical science basis:*  
634 *contribution of Working Group I to the Fourth Assessment Report of the*  
635 *Intergovernmental Panel on Climate Change*. Cambridge University Press, Cambridge;  
636 New York

637 Trebin FA (1945) *Permeability to oil of sandstone reservoir*. Gostoptekhizdat, Moscow

638 Turpening R, Toksöz M, Born A, al. e (1992) *Reservoir delineation consortium annual report*,  
639 *Massachusetts Institute of Technology, Cambridge*

640 Van Genuchten MT (1980) A closed-form equation for predicting the hydraulic conductivity of  
641 unsaturated soils. *Soil Sci Soc Am J* 44(5):892-898.  
642 doi:10.2136/sssaj1980.03615995004400050002x

643 Zhang Y, Oldenburg CM, Finsterle S (2010) Percolation-theory and fuzzy rule-based probability  
644 estimation of fault leakage at geologic carbon sequestration sites. Environ Earth Sci  
645 59(7):1447-1459. doi:10.1007/s12665-009-0131-4

646 Zhou Q, Birkholzer JT, Mehnert E, Lin Y-F, Zhang K (2009) Modeling basin- and plume-scale  
647 processes of CO<sub>2</sub> storage for full-scale deployment. Ground Water 48(4):494-514.  
648 doi:10.1111/j.1745-6584.2009.00657.x

649 **List of captions from Tables and Figures**

650

651 **Table 1** Hydro-geomechanical parameters

652

653

654 **Table 2** Parameters used for the generation of caprock fields. All considered scenarios are  
655 assumed to have a correlation length  $l_{k_1}=1,000$  m for facies 1

656

657 **Fig. 1** Representation of the clustering approach. In this example, the number of 84 inclusions-  
658 blocks (in orange) is reduced to 16 clusters (black circles). Limit of the hydrocarbon reservoir  
659 (red gridblocks) is shown by the blue line (Brown Niagaran pinnacle in Fig. 3)

660

661 **Fig 2.** Flow chart of the methodology

662

663 **Fig. 3** Cross-section of the Michigan Basin test site proposed for GCS (Turpening et al., 1992).  
664 The candidate formation is highlighted in yellow and the caprock is colored in green

665

666 **Fig. 4** Locations of 60 passive wells that cross the candidate GCS formation of the Michigan  
667 Basin (black crosses) and of the 20 equivalent clusters (blue circles). The red dot indicates the  
668 position of the proposed injection well (Merit 1-20A in Fig. 3)

669

670 **Fig. 5** Panels **a** and **b**: caprock permeability for two representative realizations of scenario 3.1.  
671 Panels **c** and **d**: ECLIPSE and ELSA-IGPS comparison of CO<sub>2</sub> mass leakage over time for  
672 realizations in **a** and **b**, respectively

673

674 **Fig. 6** CDFs of % $M_{leak}$  for ELSA-IGPS (in red) and ECLIPSE (blue) of scenario 2.1 and scenario  
675 4.1

676

677 **Fig. 7 a** Relationship between correlation length and the average distance between cluster centers  
678 and injection well and **b** relationship between correlation length and the inclusion ratio

679

680 **Fig. 8** CDF of % $M_{leak}$  for several scenarios described in Table 2

681

682 **Fig. 9** Maps of the 95<sup>th</sup> percentile of % $M_{leak}$  as a function of the injection formation permeability  
683 ( $k_{l_1}$ ) and the inclusions permeability ( $k_2$ ) for **a** scenario 1.1, **b** scenario 2.1, **c** scenario 3.1, **d**  
684 scenario 4.1, and **e** scenario 5.1

685

686 **Fig. 10** CDF of % $M_{leak}$  for some scenarios characterized by different probability  $P_2$  and the same  
687 correlation length in the cases where uncertainty in passive well is (solid lines) and is not (dashed  
688 lines) accounted for

689

690 **Fig. 11** CDFs of % $M_{leak}$  for scenarios 2.1 to 2.4 in Table 2, characterized by the same probability  
691  $P_2$  and different correlation lengths when uncertainty in passive well is (solid lines) and is not  
692 (dashed lines) considered

693

694

695 **Table 1** Hydro-geomechanical parameters

Parameter	Symbol	Value	Units
Brine density	$\rho_b$	1,045	kg m <sup>-3</sup>
CO <sub>2</sub> density	$\rho_c$	575	kg m <sup>-3</sup>
Brine viscosity	$\mu_b$	4.5×10 <sup>-4</sup>	Pa s
CO <sub>2</sub> viscosity	$\mu_c$	4.6×10 <sup>-5</sup>	Pa s
System compressibility	$c_{eff}$	4.6×10 <sup>-10</sup>	Pa <sup>-1</sup>
Injected aquifer porosity	$\varphi_{l_1}$	0.084	/
Overlying aquifer porosity	$\varphi_{l_2}$	0.05	/
Brine residual saturation	$s_b^{res}$	0.3	/
End-point CO <sub>2</sub> relative permeability	$k_{r,c0}$	0.42	/
Injection aquifer permeability	$k_{l_1}$	2.8×10 <sup>-14</sup>	m <sup>2</sup>
Overlying aquifer permeability	$k_{l_2}$	9.6×10 <sup>-15</sup>	m <sup>2</sup>
Sealing formation permeability	$k_1$	0	m <sup>2</sup>
Weak areas/inclusions permeability	$k_2$	2.8×10 <sup>-14</sup>	m <sup>2</sup>

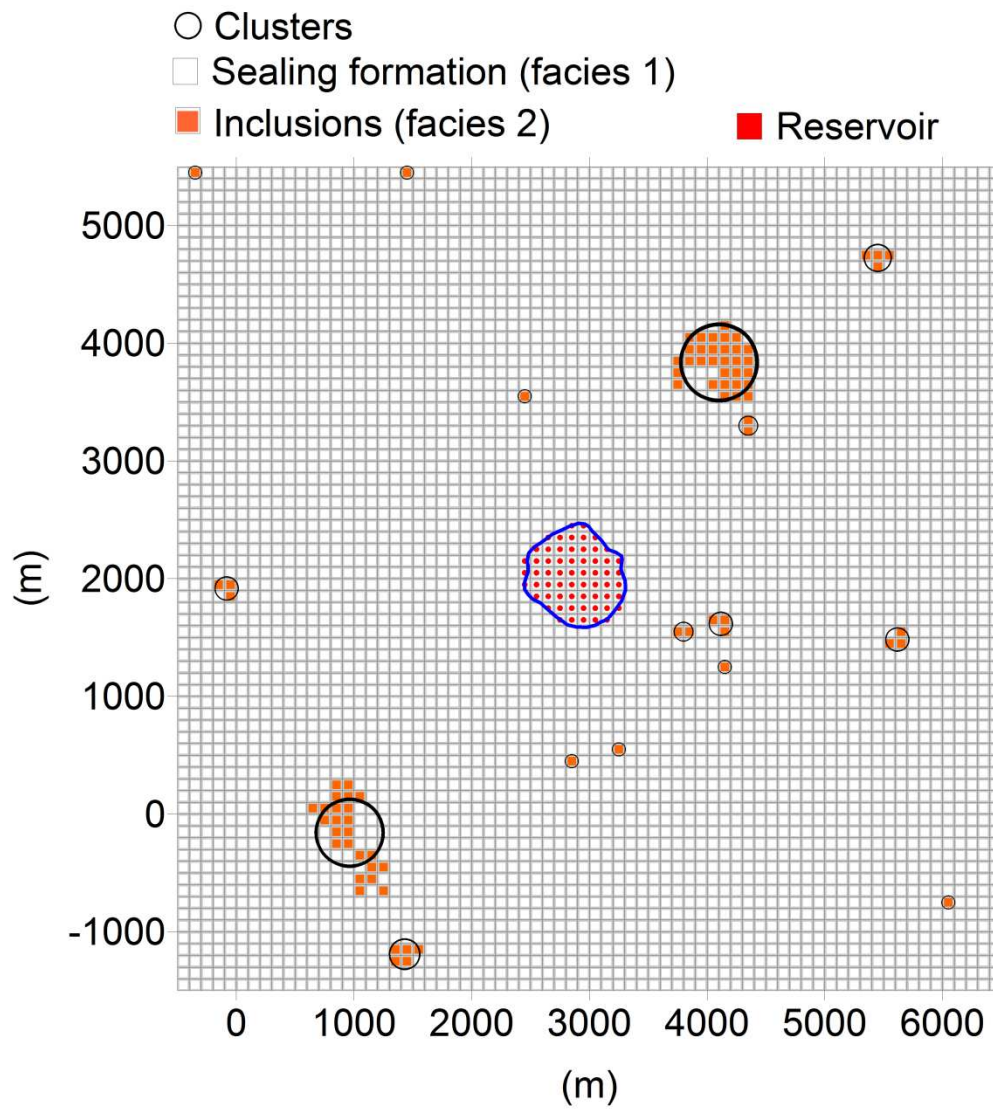
696

697 **Table 2** Parameters used for the generation of caprock fields. All considered scenarios are  
 698 assumed to have a correlation length  $l_{k_1}=1,000$  m for facies 1

Scenario	Covariance model	$N_{MC}$	$P_2^*$	$l_{xy}$ (m)
1.1	Exponential	500	0.0005	200
1.2				400
1.3				600
1.4				1,500
2.1	Exponential	500	0.001	200
2.2				400
2.3				600
2.4				1,500
3.1	Exponential	500	0.005	200
3.2				400
3.3				600
3.4				1,500
4.1	Exponential	500	0.01	200
4.2				400
4.3				600
4.4				1,500
5.1	Exponential	500	0.02	200
5.2				400
5.3				600
5.4				1,500

699 \*Facies 2 corresponds to inclusions. Probability of facies 1 (perfectly sealing formation) is  $P_1 =$   
 700  $1 - P_2$ .

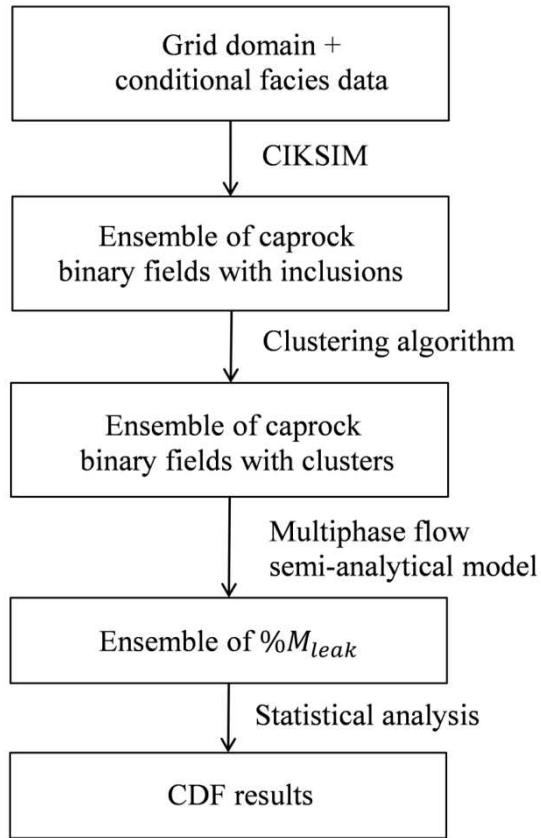
701



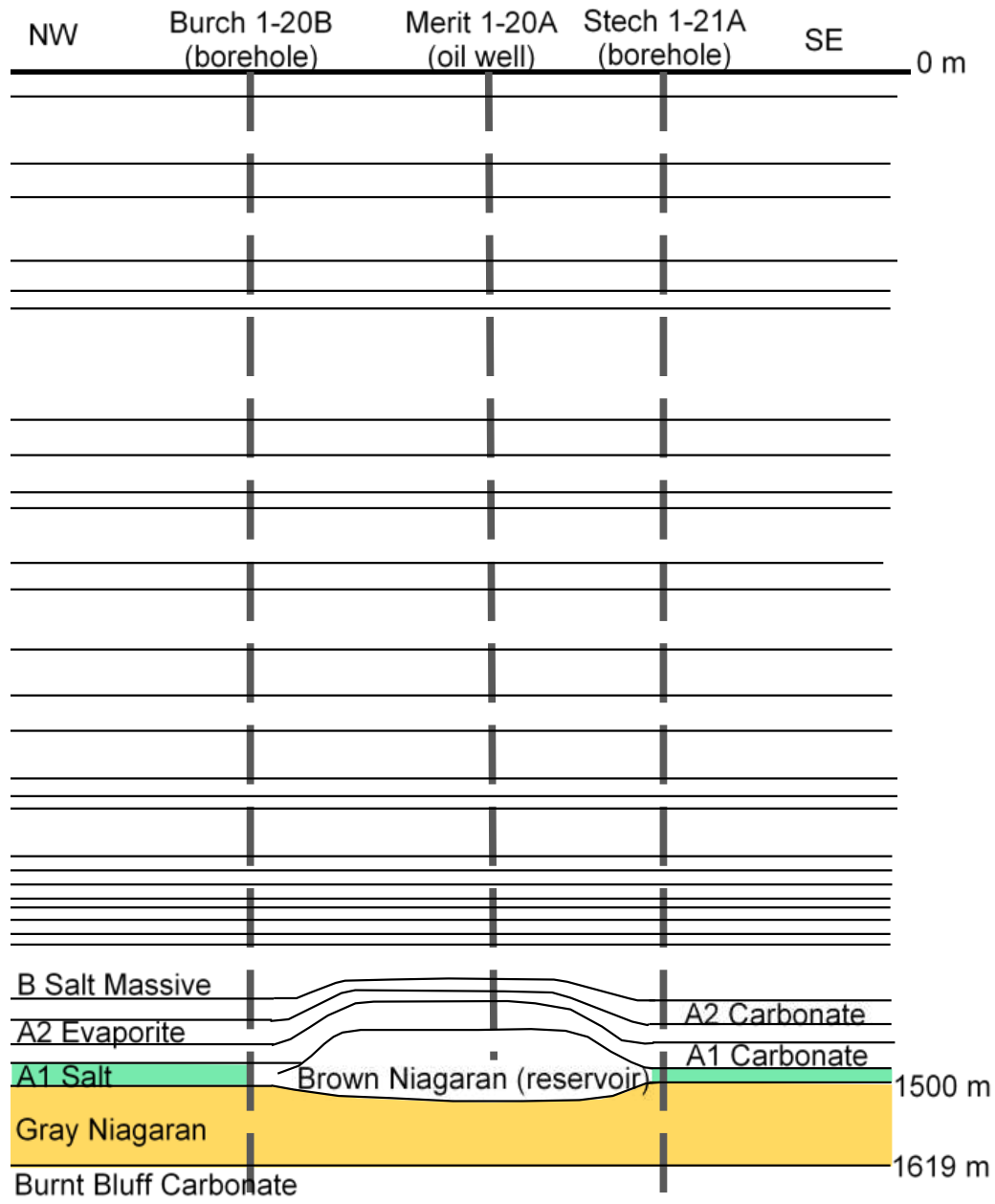
702

703 **Fig. 1** Representation of the clustering approach. In this example, the number of 84 inclusions-  
 704 blocks (in orange) is reduced to 16 clusters (black circles). Limit of the hydrocarbon reservoir  
 705 (red gridblocks) is shown by the blue line (Brown Niagaran pinnacle in Fig. 3)

706



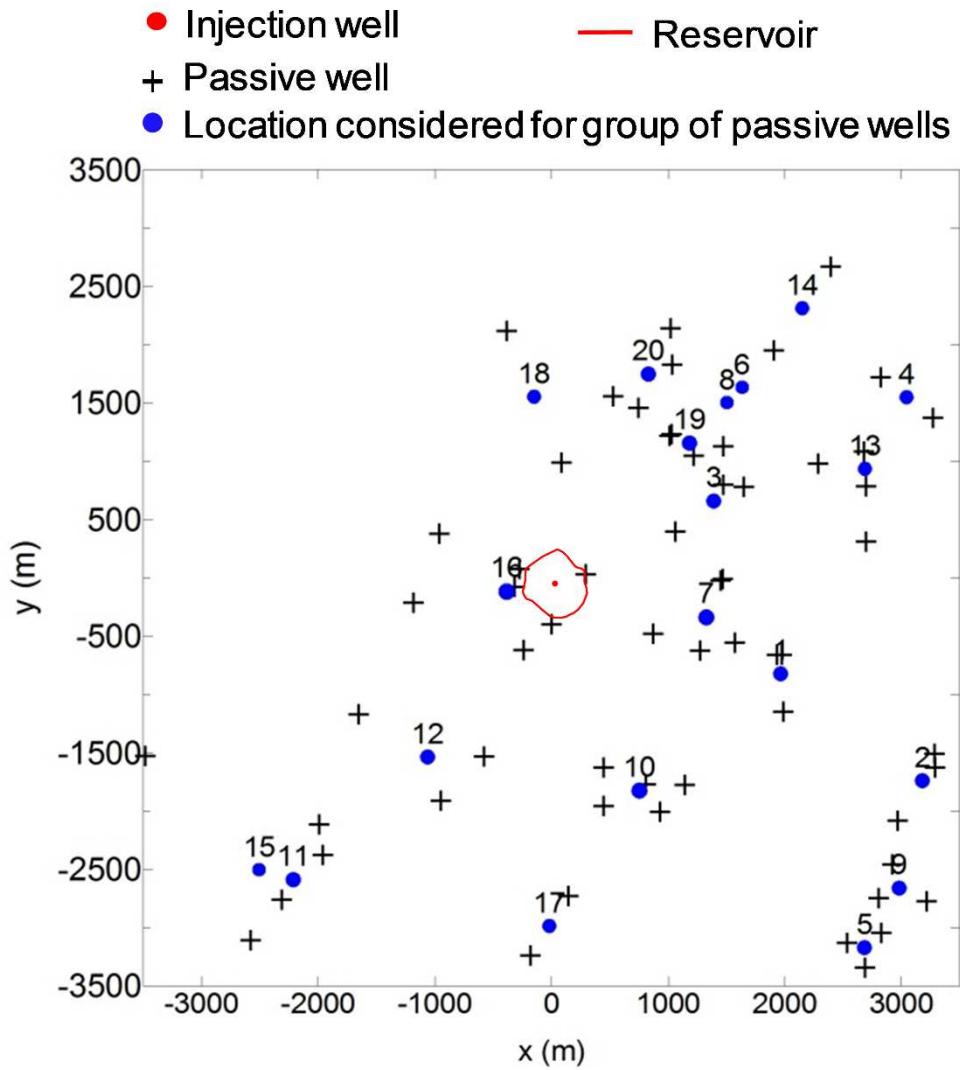
707  
708 **Fig 2.** Flow chart of the methodology



709

710 **Fig. 3** Cross-section of the Michigan Basin test site proposed for GCS (Turpening et al., 1992).

711 The candidate formation is highlighted in yellow and the caprock is colored in green



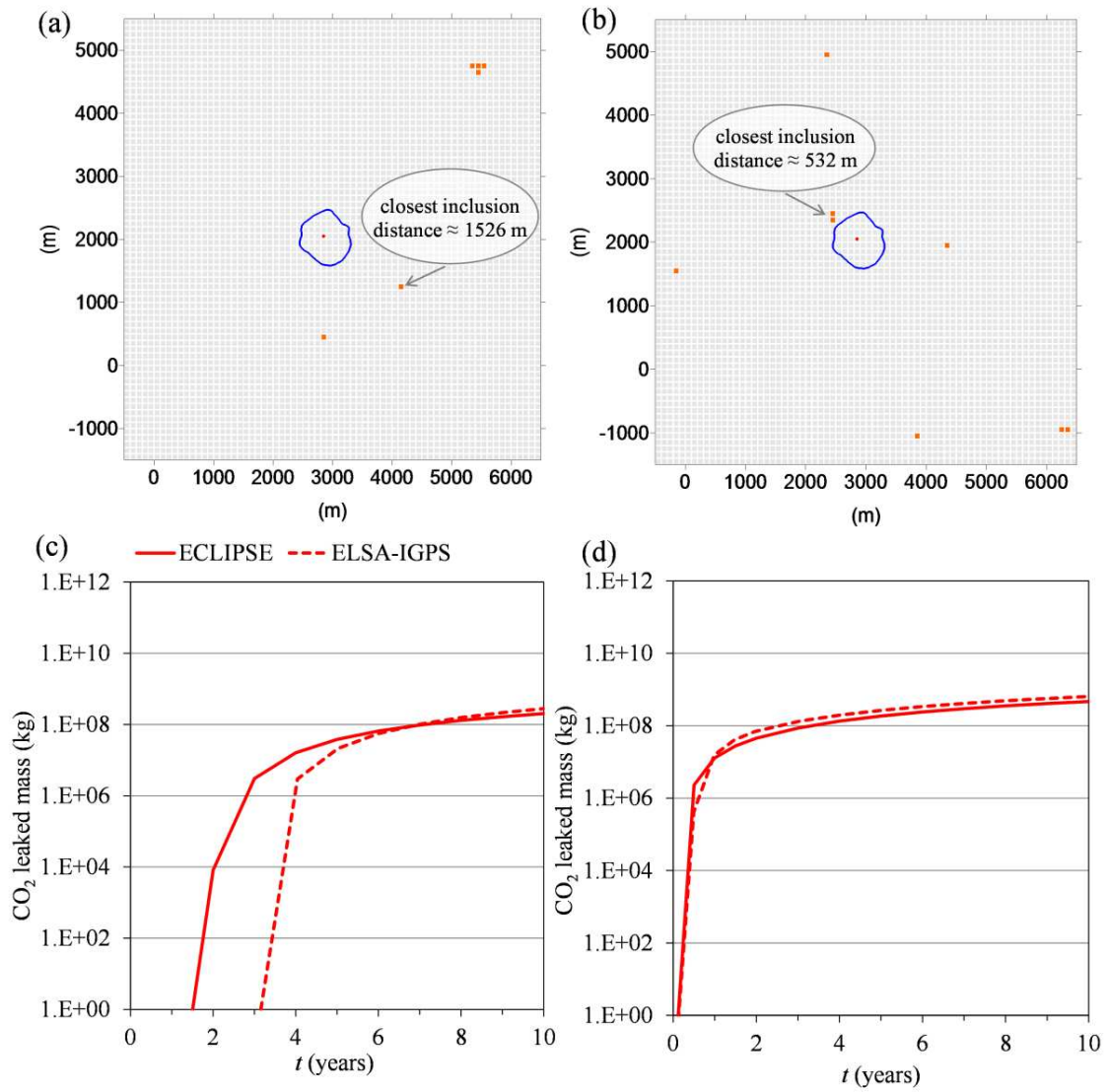
712

713 **Fig. 4** Locations of 60 passive wells that cross the candidate GCS formation of the Michigan

714 Basin (black crosses) and of the 20 equivalent clusters (blue circles). The red dot indicates the

715 position of the proposed injection well (Merit 1-20A in Fig. 3)

716



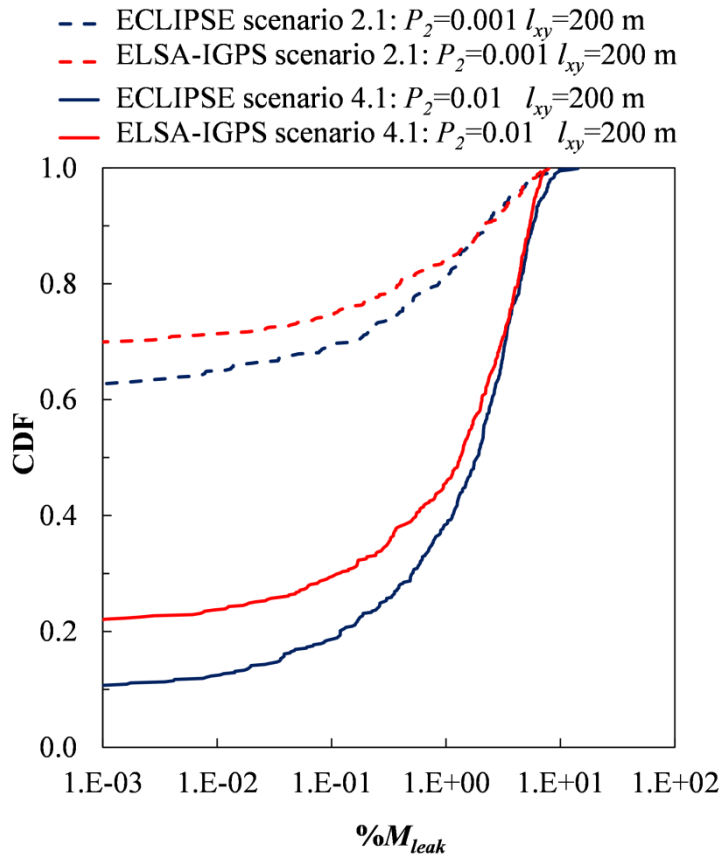
717

718 **Fig. 5** Panels **a** and **b**: caprock permeability for two representative realizations of scenario 3.1.

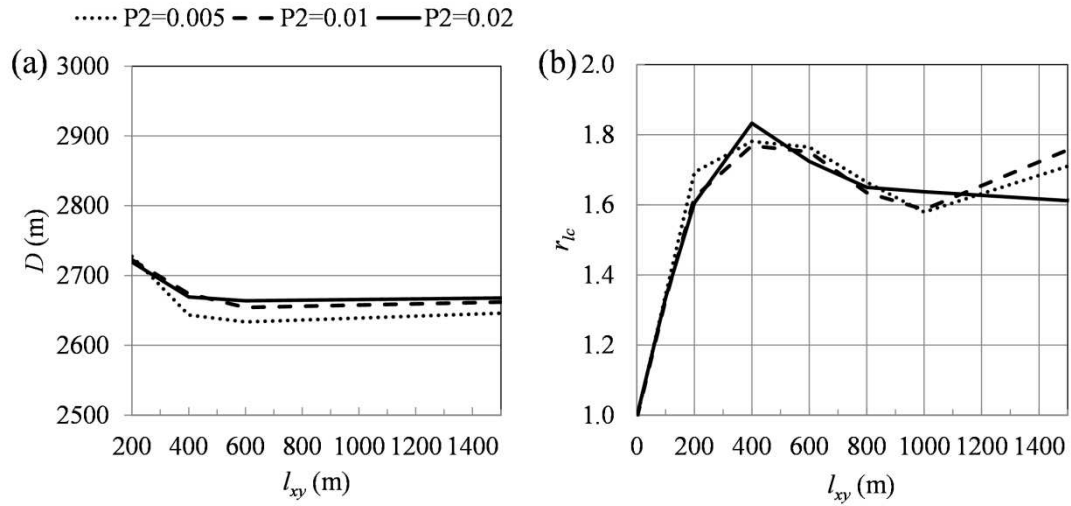
719 Panels **c** and **d**: ECLIPSE and ELSA-IGPS comparison of CO<sub>2</sub> mass leakage over time for

720 realizations in **a** and **b**, respectively

721



722  
 723 **Fig. 6** CDFs of  $\%M_{leak}$  for ELSA-IGPS (in red) and ECLIPSE (blue) of scenario 2.1 and scenario  
 724 4.1  
 725



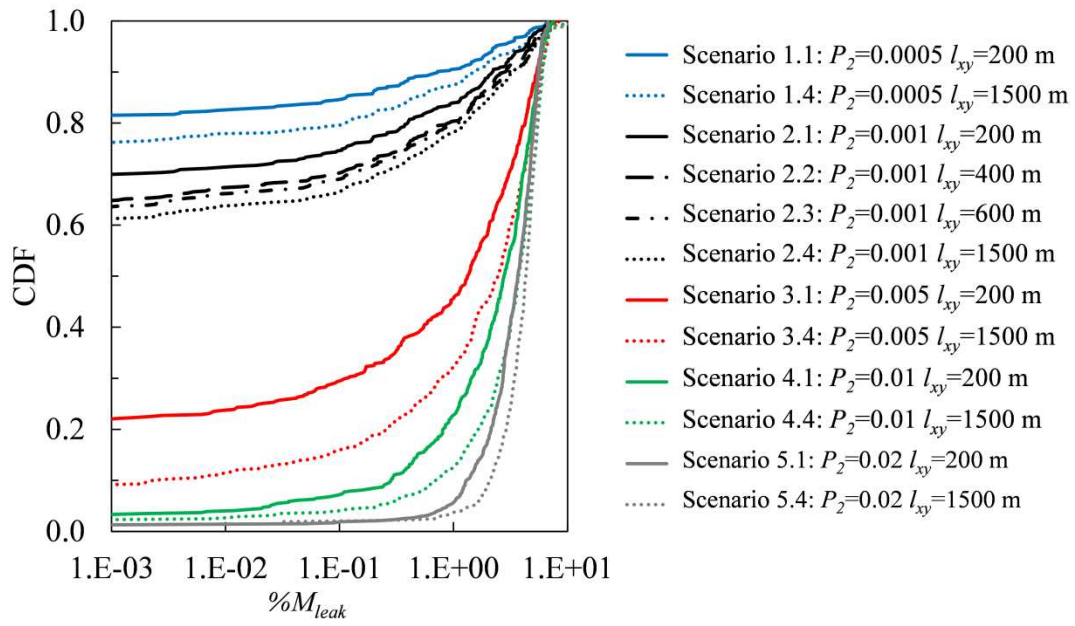
726

727 **Fig. 7 a** Relationship between correlation length and the average distance between cluster centers

728 and injection well and **b** relationship between correlation length and the inclusion ratio

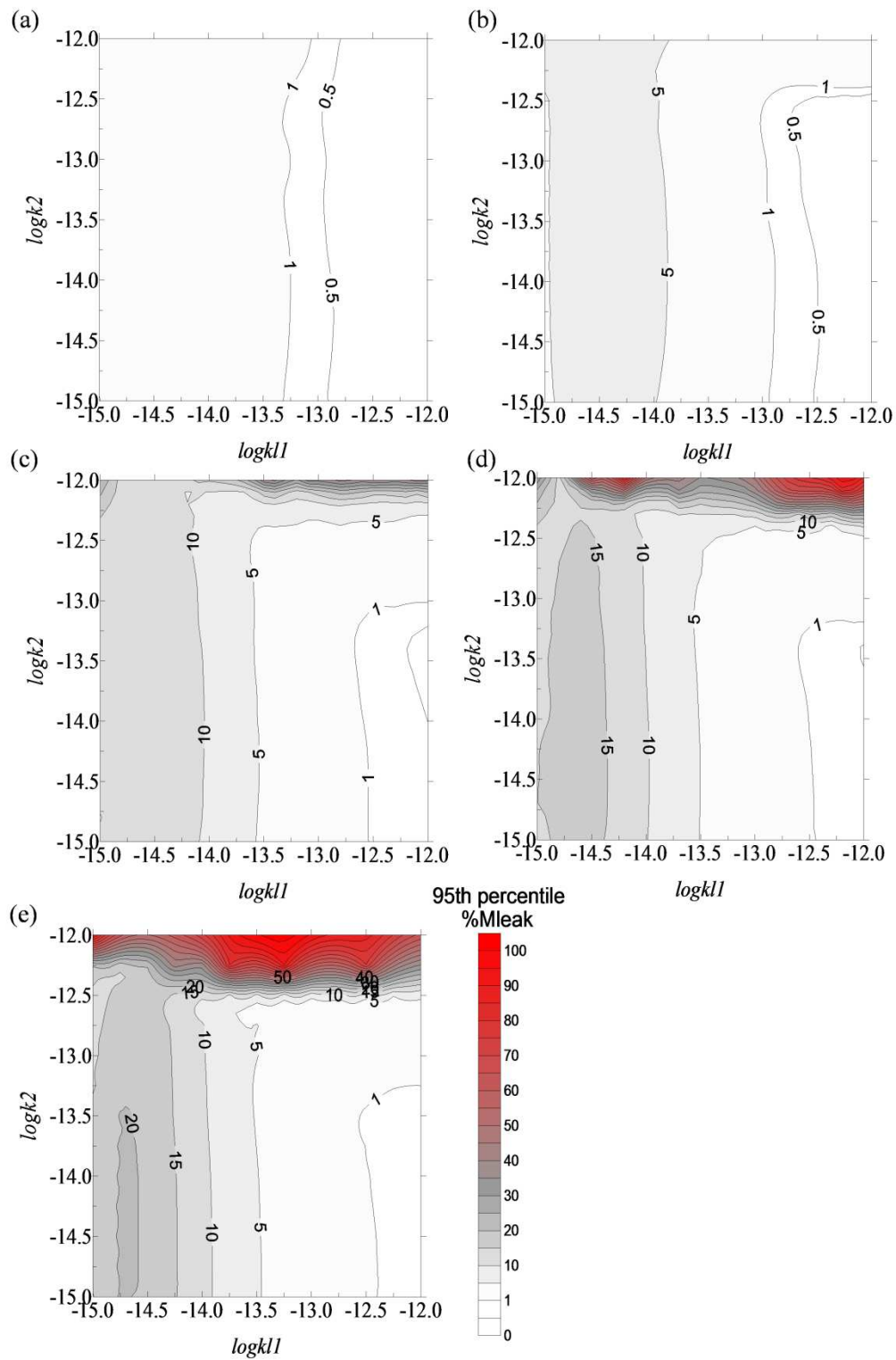
729

730



732 **Fig. 8** CDF of %M<sub>leak</sub> for several scenarios described in Table 2

733



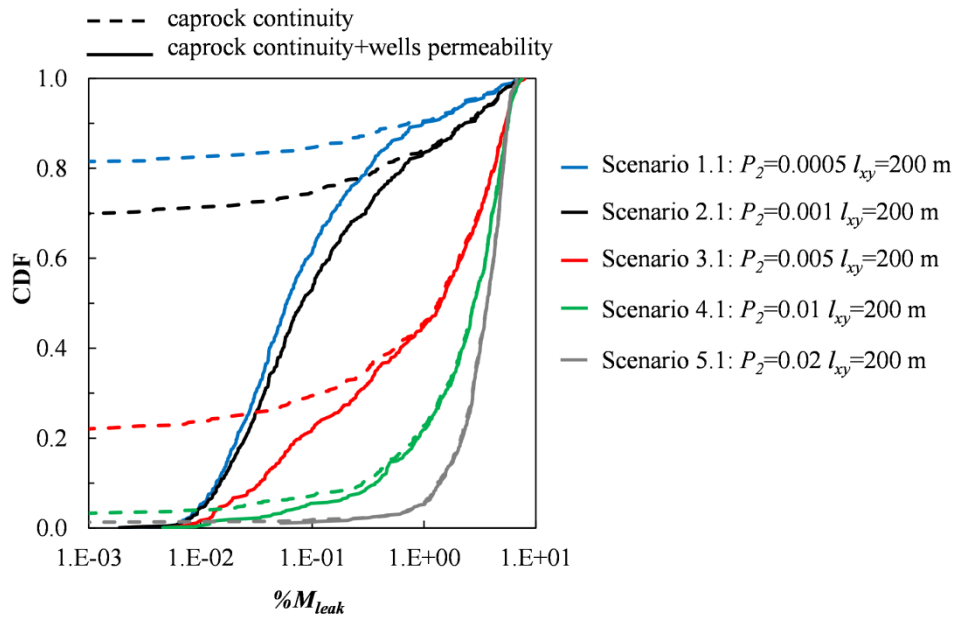
734

735 **Fig. 9** Maps of the 95<sup>th</sup> percentile of  $\%M_{leak}$  as a function of the injection formation permeability

736 ( $k_{l1}$ ) and the inclusions permeability ( $k_2$ ) for **a** scenario 1.1, **b** scenario 2.1, **c** scenario 3.1, **d**

737 scenario 4.1, and **e** scenario 5.1

738



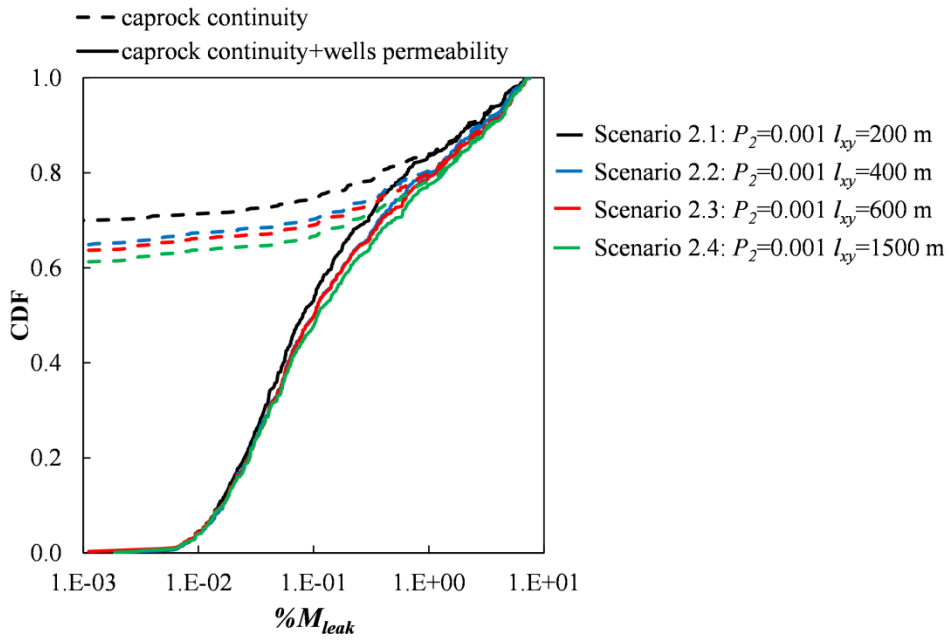
739

740 **Fig. 10** CDF of  $%M_{leak}$  for some scenarios characterized by different probability  $P_2$  and the same  
741 correlation length in the cases where uncertainty in passive well is (solid lines) and is not (dashed  
742 lines) accounted for

743

744

745



746

747 **Fig. 11** CDFs of  $\%M_{leak}$  for scenarios 2.1 to 2.4 in Table 2, characterized by the same probability

748  $P_2$  and different correlation lengths when uncertainty in passive well is (solid lines) and is not

749 (dashed lines) considered

750

751